International Journal of Engineering and Geosciences
https://dergipark.org.tr/en/pub/ijeg
e-ISSN 2548-0960

Spatio-Temporal monitoring of Qeshm mangrove forests through machine learning classification of SAR and optical images on Google Earth Engine

Mostafa Mahdavifard[1], Sara Kaviani Ahangar[2], Bakhtiar Feizizadeh[*1], Khalil Valizadeh Kamran[1], Sadra Karimzadeh[1]

[1]*University of Tabriz, Department of Remote Sensing and GIS, Iran*
[2]*University of Hormozgan, Department of Combat Desertification, Iran*

Keywords
Mangrove
Machine learning Algorithm
Google Earth Engine
Remote Sensing
Qeshm Island

Research Article
DOI: 10.26833/ijeg.1118542

Received:18.05.2022
Revised: 14.04.2023
Accepted:19.04.2023
Published:08.05.2023

Abstract

Mangrove forests are considered one of the most complex and dynamic ecosystems facing various challenges due to anthropogenic disturbance and climate change. The excessive harvesting and land-use change in areas covered by mangrove ecosystems is critical threats to these forests. Therefore, the continuous and regular monitoring of these forests is essential. Fortunately, remote sensing data has made it possible to regularly and frequently monitor this forest type. This study has two goals. Firstly, it combines optical data of Landsat- 8 and Sentinel-2 with Sentinel-1 radar data to improve land cover mapping accuracy. Secondly, it aims to evaluate the SVM machine learning algorithms and random forest to detection and differentiate forest cover from other land types in the Google Earth Engine system. The results show that the support vector machine (SVM) algorithm in the S2 + S1 dataset with a kappa coefficient of 0.94 performs significantly better than when used in the L8 + S1 combination dataset with a kappa coefficient of 0.88. Conversely, the kappa coefficients of 0.89 and 0.85 were estimated for the random forest algorithm in S2 + S1 and L8 + S1 datasets. This again indicates the superiority of Sentinel-2 and Sentinel-1 datasets over Landsat- 8 and Sentinel-1 datasets. In general, the support vector machine (SVM) algorithm yielded better results than the RF random forest algorithm in optical and radar datasets. The results showed that using the Google Earth engine system and machine learning algorithms accelerates the process of mapping mangrove forests and even change detection.

1. Introduction

Mangrove forests are swampy plant communities located in tropical regions between sea and land on tropical and subtropical coastlines [1-2]. These forests are prolific ecosystems with significant ecological and economic consequences [3-4]. Mangrove forests help reduce coastal flooding and erosion and protect inland farms, livestock and aquaculture, and other coastal communities against natural hazards such as tornadoes and storms [5]. However, these forests are at high risk due to rapid population growth, poor planning, and unbalanced economic development. The increasing problems related to mangrove forests worldwide are serious issues faced by coastal ecosystems. Unfortunately, these forests are affected by human habitats, pollution, storms, and sea waves [6]. In Iran, this type of forest is under threat due to the following factors: excessive harvesting in the branches of these forests, road development, the improper establishment of industries, forest use without proper recreational planning, pollution caused by oil hydrocarbons, increasing aquaculture activities and the general lack of environmental mechanisms in these forests [7].

It is impossible to monitor mangrove forests traditionally since they are located in intermedia areas [8]. Meanwhile, satellite remote sensing data can be used for large areas over time so that this technology can be used as an alternative to mangrove forest monitoring. Many researchers have mapped mangrove forests worldwide, using various satellite remote sensing data, including optical images [9-10] and SAR [11]. Mangrove forests can be monitored on a large scale, using high-resolution spatial images (less than 1 meter), such as

* **Corresponding Author**

(mostafamahdavi842@gmail.com) ORCID ID 0000-0001-9811-5428
(sarakaviani11@gmail.com) ORCID ID 0000-0003-0382-1480
*(feizizadeh@tabrizu.ac.ir) ORCID ID 0000-0002-3367-2925
(valizadeh@tabrizu.ac.ir) ORCID ID 0000-0003-4648-842X
(sadra.karimzadeh@gmail.com) ORCID ID 0000-0002-5645-0188

Cite this article

Mahdavifard, M., Ahangar, S. K., Feizizadeh, B., Kamran, K. V., & Karimzadeh, S. (2023). Spatio-Temporal monitoring of Qeshm mangrove forests through machine learning classification of SAR and optical images on Google Earth Engine. International Journal of Engineering and Geosciences, 8(3), 239-250

Worldview, Quickbird, and aerial photographs; however, due to cost constraints, data volume used by users is limited. As a result, freely accessible satellite images (e.g., Landsat-8 and Sentinel-2) and medium spatial resolution (30 and 10 m) are widely used for extracting data of large-scale mangrove forests [12]. Continuous cloud coverage and inundation of tidal lands in coasts prevent access to high-quality optical data [13-15]. With the advent of Sentinel-1 C-band synthetic aperture radar images, it is possible to provide land cover classifications in repetitive, cloud-covered environments [16]. SAR plays an essential role in monitoring the biophysical parameters of mangrove forests since its microwave energy can penetrate cloud masses formed continuously in tropical regions, making it possible to obtain data throughout the year [17]. Combining optical and SAR data can improve classification accuracy, contributing significantly to the protection of mangrove forests. This type of data combination provides more detailed information for studying the spatial distribution and dynamic changes of mangrove forests, which play an essential role in developing conservation and management policies [18]. The increase in the number of sensors and free satellite data has led to new platforms that help users select and process large volumes of spatial data. Google Earth Engine (GEE) is an excellent example of a cloud-based computing platform that provides easy access to satellite data sets on a planet-scale [19-20]. For example, GEE provides free preprocessed satellite series data (including Landsat-, Sentinel-2, and Sentinel-1), along with the required disk space and advanced machine learning classification algorithms [1]. The online GEE system offers more than 15 classification techniques, with most studies conducted rely on machine learning algorithms [21-22] CART, RF, and SVMs. This is because these methods have proved to be some powerful ways to classify land cover. Such methods based on free data and robust algorithms can be helpful for regular monitoring [23]. So far, many studies have been done on mangrove forests using optical and radar remote sensing methods worldwide. In West Africa, mangrove forests were mapped using machine learning algorithms in Google Earth and Sentinel-2 images, with thematic maps found to have an accuracy of 90% [23]. A comparative study to differentiate mangrove forests from non-mangrove forests using NDVI, NDWI, SAVI indices, SR, and CMRI showed that the combined CMRI index has better accuracy than other indicators used [5]. Multimodal mapping of mangrove forests in China showed that integrating RADARSAT-2 polarization data and Landsat-8 data can increase the overall accuracy (OA) by 95%, while optics classification alone can produce an OA of about 83% [18]. A study integrating Sentinel-2 multispectral time-series images with Sentinel-1 images for mapping Spartina alterniflora and Mangrove in Zhangjiang Est showed that the 10-meter maps produced represented a relatively stable spatial pattern mangrove and rapid expansion Spartina alterniflora [24]. Another study using Landsat- 8 multidimensional data to map and identify mangrove changes in Pong Vietnam showed that Landsat- multidimensional data, along with image segmentation and GIS approaches, has a high potential to map mangrove forests in the coastal area [25]. Three spectral criteria (spectral match degree (SMD), normalized difference mangrove index (NDMI), and shortwave infrared absorption) were found to better differentiate mangrove forests from other vegetation in Landsat- images 8. The results showed that using spectral criteria (UA = 85%, PA = 94%, OA = 95%) is better than using raw band reflectance data (UA = 72%, PA = 82). ٪, OA = 90%) [26]. the changes in mangrove forests around Trat Province in Thailand were mapped by analyzing and processing 3-decade images via the GEE Web System. The results show that the use of a web-based monitoring system of GEE contributes to mapping and preserving the coastal ecosystems [27]. .Hu et al[12] used Sentinel-1 and Sentinel-2 time-series data in Google Earth Engine in China to map mangrove forests on a national scale. The results showed the significant capability of Sentinel-1 and Sentinel-2 images in producing accurate maps of mangrove forests with high resolution in GEE. Producing accurate thematic maps of mangroves with Sentinel 1 and Sentinel 2 data is important and necessary for planners. The result showed an increase in overall accuracy and kappa coefficient [28]. Ghorbanian et al. [29] used the combination of Sentinel 1 and Sentinel 2 images to create a functional index. The results of the researchers showed that the performance of the combined index was good in mangrove identification and it is widely used in large-scale mangrove mapping. In a study, the combination of optical and star data was used for mangrove mapping. The results showed that the combination of optical and SAR data can effectively improve the classification accuracy [30]. The present study uses the Cloud Google Earth Engine to monitor and map the Qeshm mangrove forests (southern Iran), which are designated as protected forests. The first purpose of this study was to combine images obtained from optics and radar (Sentinel-2 and Sentinel-1- Landsat-8 and Sentinel-1) systems with a different spatial resolution to compare them in terms of the accuracy of resulting thematic maps. The second purpose of this study was to compare and evaluate the performance of two algorithms, namely, SVM and RF machine learning, to identify mangrove forests and differentiate them from other land covers in the combined optics and radar images in the Google Earth Engine cloud platform. In previous studies, Sentinel-2 and Landsat-8 with optical nature were not integrated with Sentinel 1 SAR satellite with radar nature, which is superior to previous studies in the present study, and two RF and SVM machine learning classifiers were used simultaneously.

2. Material, Method and Case studies

2.1. Case studies

The case study is the mangrove forest in Hormozgan province in Iran (Figure 1a). Qeshm Island, with an area of approximately 1.491 square kilometers, is the largest island in the Persian Gulf and 2.5 times the size of Bahrain. Mangrove forests are located between Khamir City and Qeshm Island between latitude 26.45 ° - 27.00 ° and longitude 55.20 ° - 55.51 ° (Figure 1b). Figure 1c

shows the map of land cover in the protected mangrove area. These forests account for the largest area of forests in Iran and even in the Persian Gulf countries, covering 85% of Iranian mangroves. The majority of the mangrove forest cover in this area includes Avincina or mangrove. The mangrove biosphere has an area of 20 by 20 km, where several tidal channels have been identified [31].

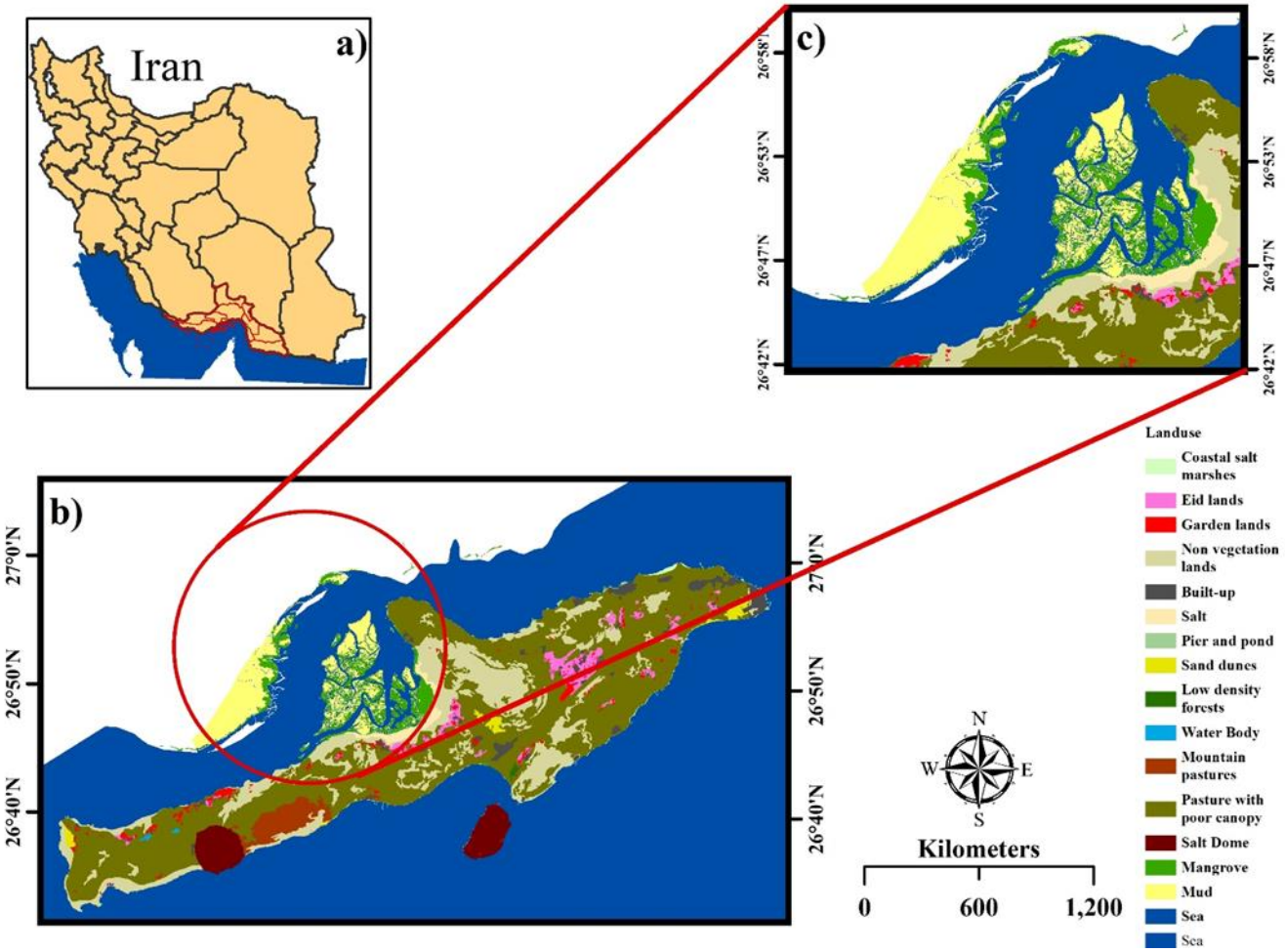

Figure 1. The geographical Location, Hormozgan Province in Iran (a), updated land use map of Qeshm Island (b), the land use map of the mangrove forests in the study area (c)

2.2. Data

2.2.1. Reference data

In this study, three datasets are as reference data. The land-cover map of the study area, global mangrove data [32], and high-resolution images obtained by Google Earth. To create a single data, the national land cover map was updated with global mangrove data in open-source QGIS software and was used as reference data and high-resolution Google Earth Images to choose validation samples. Samples of water classes and tidal areas were selected and collected from Google Earth photos, while samples of mangrove and mud classes were taken from the updated land cover map.

2.2.2. Satellite data

Launched on February 11, 2013, the Landsat-8 satellite is one of the new multispectral satellites, imagining the entire Earth every 16 days. This satellite has two OLI sensors and an infrared thermal sensor (TIRS). The Landsat-8 satellite has 11 spectral bands in the visible range, reflected infrared and thermal infrared with 15-, 30-, and 100-meters spatial resolution. The second satellite of the Sentinel series is called Sentinel-2, which began its operation on June 23, 2015. The Sentinel-2 satellite includes two Sentinel-2A and Sentinel-2B twin satellites. This satellite has 13 spectral bands in the visible range, near-infrared, and middle infrared with different resolutions of 10, 20, and 60 meters. Although this satellite is twin, its spatial resolution has been reduced to 5 days compared to the Landsat--8 satellite, which is unique.

Sentinel-1 is one of the Sentinel-satellites series that falls in the radar category, capturing the image of the Earth in the C band at two polarities VV and VH. This satellite has a spatial resolution of 5 to 20 meters per Azimuth and, like the Sentinel-2 optical satellite, has two types, A and B, which have reduced the review period of this satellite to 5 days.

This study uses the following: the average series images of monthly cloud-free combination (all months of 2016 except May due to severe cloudiness), Sentinel-2 Level1C atmosphere reflection in Google Earth Engine (ee.ImageColection ID: COPERNICUS / S2), monthly time series images of a cloud-free combination of Landsat-8

for the high reflection atmosphere in Google Earth Engine (ee.ImageColection ID: LANDSAT- / LC8 / C01 / T1_TOA) as well as GRD Sentinel-1 monthly time series images in Google Earth Engine (ee.ImageColection ID: COPERNICUS / S1). Many researchers have suggested VH polarization to monitor land cover [33-34], so in this study, the Backscatter value of VH polarization was used. Table 1 describes the data used.

Table 1. Characteristics of satellite data

Satellite	Landsat-8	Sentinel-2	Sentinel-1
Sensor (type)	OLI (Optical)	MSI (Optical)	SAR (Radar)
Data Level	Level 1	Level 1C	GRD
Spectral Band/ Polarization (um)	B3 (560) B4 (660) B5 (865)	B3 (560) B4 (665) B8 (842)	C-VH (5.62 cm)
Spatial Resolution (m)	30	10	5 * 10
Repeat Frequency (days)	16	5	6
Time Series	2016/1/1 – 2017/1/1		

2.3. Methods

As shown in the procedure flowchart (Figure 2), the spectral indices were initially calculated separately based on the time series satellite images in the Google Earth Engine system (Landsat-8 and Sentinel-2). Secondly, the spectral indices used for each satellite were combined with the series images Sentinel-1 and placed in a dataset. Third, the mangrove forest cover was mapped using machine learning classification algorithms (RF and SVM) in GEE. Finally, to evaluate the classified maps, they were compared with the reference data.

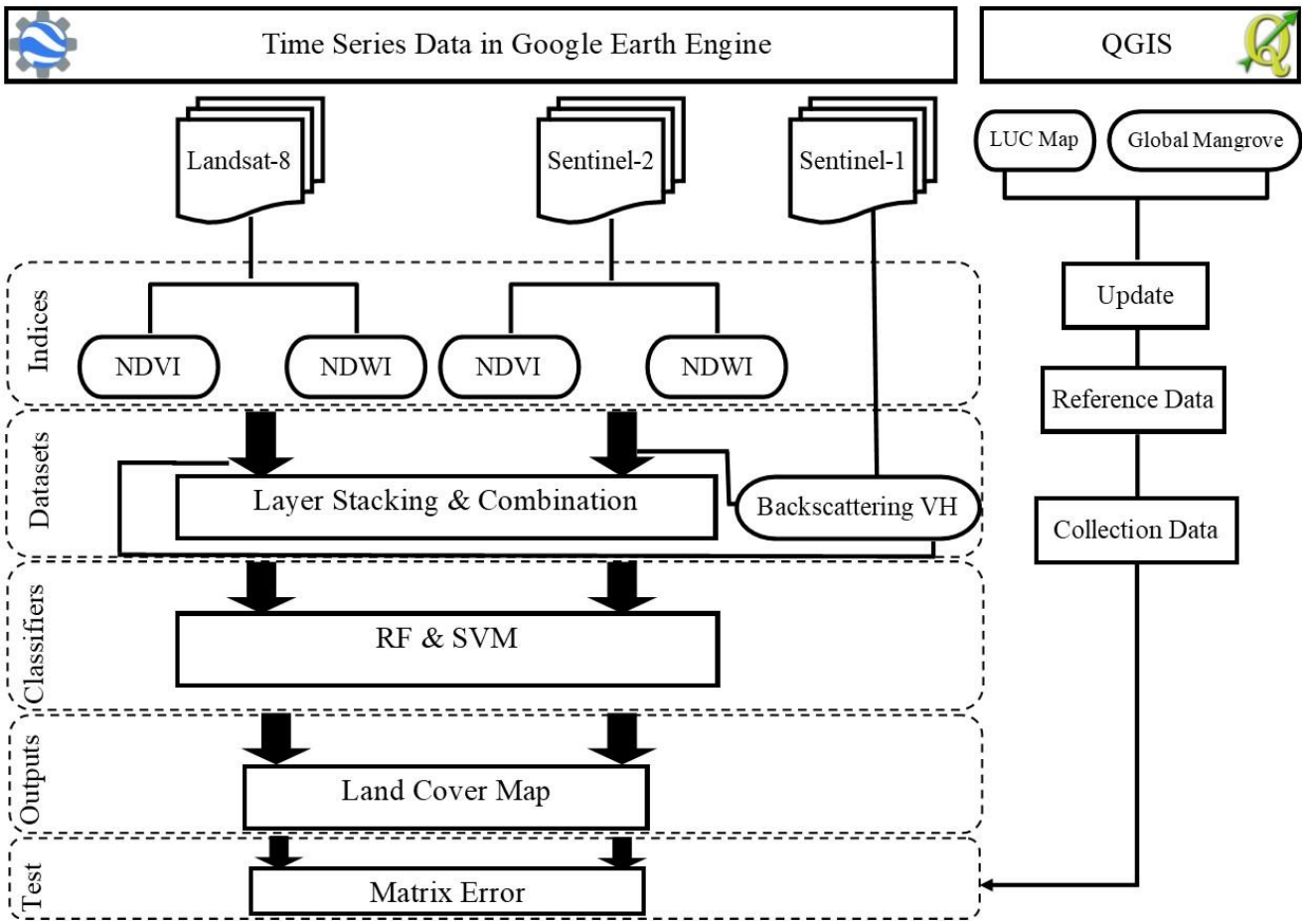

Figure 2. Research flowchart

2.3.1. Calculation of NDVI Time-Series

The present study detects and differentiates mangrove jungles from other vegetation and land, using the Normalized Differential Vegetation Index (NDVI). NDVI index was applied separately to the Sentinel-2 and Landsat-8 multispectral time-series images in Google Earth Engine. NDVI is one of the most common indicators used for vegetation dynamics at a regional and global scale [35-36]. This index developed by [37] (T) is calculated based on the ratio between the TOA reflectivity of the red band in the spectral range of 0.66

μm and the near-infrared band (NIR) in the range of 0.86 μm [38]. The value of NDVI ranges from - 1 to 1. Low NDVI values indicate vegetation under moisture pressure, and higher values indicate a higher level of green vegetation density [39-40]. This index is calculated based on Equation 1:

$$NDVI = \frac{NIR - Red}{NIR + RED} \quad (1)$$

NIR represents the near-infrared band in the spectral range of 865 and 842 nm, and the red band ranges from 660 to 665 nm.

2.3.2. Calculation of NDWI Time-Series

Given the presence of water canals in the mangrove-covered area, water canals were identified and differentiated from other water bodies using the NDWI Normalized Differential Index in GEE. To this end, this index was calculated on time-series images (Landsat- 8 and Sentinel-2) to identify water channels. NDWI index is the best indicator for mapping water size. It is also a suitable index for monitoring the hydrological condition of wetlands. The value of NDWI ranges from 1 and-1, with negative values or near negative and positive values representing a water area with high humidity. NDWI was calculated using Equation 2 [41]:

$$NDWI = \frac{Green - NIR}{Green + NIR} \quad (2)$$

NIR represents the near-infrared band in the spectral range of 865 and 842 nm, Green: the green band is in the range of 560 nm.

2.3.3. Data integration and combination

After calculating the spectral indices on the satellite imagery used, all the time series indices (NDWI, NDVI from the Sentinel-2 image) and the VH polarization time series redistribution image (Sentinel-1) were stacked and integrated into a single data set. Also, all the time series indices (NDWI and NDVI) calculated for Landsat-8 and the VH Sentinel-1 polarization time series redistribution image were stacked and integrated into a single data set. The Landsat-8 and Sentinel-1 combination datasets included 33 bands (11 NDVI indices, 11 NDWI indices, and 11 VH redistribution images), and the Sentinel-2 and Sentinel-1 combination datasets, had 33 bands. All these processes were performed in the GEE system.

2.3.4. Determining training data of classification

A total of 500 points in the area under study were selected in GEE to determine the training samples to classify four land cover classes (mangrove, tidal lands, mud, and seawater). The appropriate distribution of the samples was the primary criterion for selecting the sample. The data were collected using a combination of NDVI (Feb-Mar-Jan) and (Feb-Sep-Apr) in the images of Sentinel-2 and Landsat-8, respectively, due to unstable environmental conditions such as submersion of tidal areas. This study used a completely random sampling method based on the visual evaluation of images and the ratio of different land cover in the study area. Jensen says that classes that are more important and have more importance are sampled more [42]. So, since the main purpose of the current paper was to separate mangroves from other lands by the mentioned method, we took more samples for the main purpose, which was mangroves, and less sampling should be done for other lands. So, 200 and 100 points were collected for the mangrove class and the other three land cover classes, respectively.

2.3.5. Image classification

Machine learning algorithms have been used in remote sensing for decades (e.g., from basic algorithms such as PCA and K-Means to more complex classifications and regression frameworks such as SVMs, decision trees, random forests, and artificial neural networks [43]. It has received special attention for land use and land cover [44-45]. There are many classification algorithms, but RF and SVM were also used in this paper due to their frequency and most use in previous studies. In a study to prepare a land cover map in the GEE system, they used machine learning classifications and concluded that RF and SVM algorithms have higher accuracy than other machine learning classifications [46].

Random Forest is a non-parametric "machine learning" algorithm [47-48]. Nowadays, RF is considered one of the most widely used algorithms for land cover classification, which uses remote sensing data [49-51]. This classification method uses bootstrap aggregating or bagging to generate random vectors with N samples (N: the size of the primary input training data) and select the training data for each class [52]. Each pixel is assigned to one class based on the popular votes of all tree predictors [23].

SVM methods have also been successfully applied in various classification approaches [53-54]. SVM is a machine learning method based on Vapnik Chervonenkis's dimension theory, drawing on the principle of minimum structural risk [55]. Generally, SVM is widely used and can turn nonlinear problems into linear problems by creating a different function in high-dimensional space; therefore, it is not affected by sample dimensions and can prevent misclassification [56]. The Classifier package manages and supports machine learning algorithms in the GEE system. These classifiers include CART, Random Forest, NaiveBayes, and SVM. In this research, RF and SVM classification in the classifier package of the GEE system was used to classify land cover. For this purpose, the datasets created for each satellite (Sentinel-2 + Sentinel-1 and Landsat-8 + Sentinel-1) containing calculated spectral indices and redistribution of radar VH polarization were each separately placed as the input of RF and SVM classification algorithms. Note: 1, 50 trees were taken into account using a trial-and-error method in order to perform the RF classification for the desired result. 2-100% of the points collected in the previous stage (determination of training data) were designated as

training points in the image classification process since we had access to reference data for the validation (testing) of RF and SVM classifiers.

2.3.6. Validation

In this study, the accuracy of land cover maps obtained from the classifiers was validated, using a reference map (combination of national land cover map and global forest cover); therefore, 30 samples (for each class: mangrove, mud, tidal areas, and sea) and a total of 120 samples as a control point on the reference map were selected and determined to assess the accuracy. Researchers strongly suggest that one can't use the kappa coefficient parameter to compare and evaluate the accuracy of thematic maps obtained from image classification [50-57]. The advantage and capability of kappa coefficient is that it works well in unbalanced data. Another advantage of Kappa is that it can be used for multiple classes. Due to the unbalanced nature of the data, this coefficient is fruitful. Therefore, this study assesses the accuracy of classification methods using the optimal parameters extracted from the error matrix, such as overall accuracy (OA), producer's accuracy (PA), and user accuracy (UA). Table 2 shows the details of the assessment parameters used in this study.

Table 2. The statistical parameters of error matrix used in this study

Matrix Error	Formula	Description	Reference
Overall accuracy	$\frac{1}{N}\sum Pii$	Where OA defines the total accuracy of the model, test pixels are described by N, and P pii represents the total number of correctly classified pixels.	[58]
kappa	$\frac{N\sum_{i=1}^{r} xii - \sum_{i=1}^{r}(x_{i+} \times x_{+1})}{N^2 - \sum_{i=1}^{r}(x_{i+} \times x_{+1})}$	Where k is the number of rows (e.g., land-cover classes) in the error matrix, xii is the number of observations in row i and column i, and xi+ and x+j are the marginal totals for row i and column j, respectively, and N is the total number of samples.	
User's accuracy, UA	$\frac{x_{ii}}{x_{1+}}$	Where x_{ii} the number of correctly classified pixels is, x_{1+} is the number of pixels in a category. x_{+j} is the number of sample pixels in a category.	[42]
Producer's accuracy, PA	$\frac{x_{jj}}{x_{+j}}$		

3. Results

3.1. Mangrove phenology cycle and other vegetation

Figure 3 shows the monthly average of the NDVI time series of the Sentinel-2 and Landsat-8 satellites. The NDVI values of the mangrove cover and the typical vegetation in the Sentinel-2 images are much higher than the NDVI values calculated from the Landsat-8 images. In general, the NDVI of mangrove cover in Sentinel-2 and Landsat-8 was almost higher than that of normal vegetation per month, while the changes in typical vegetation fluctuated relatively highly per month. This factor is a distinguishing feature for identifying and differentiating mangroves from other vegetation in the area. As this figure shows, it can be concluded that spring is the best time to monitor mangrove forests in the study area (January, February, March) since the NDVI values in Landsat-8 and Sentinel-2 are 0.57 and 0.64 percent, respectively, indicating a high level of greenery of mangroves forests compare to other months of the year.

3.2. Accuracy assessment

Table 3 shows the resulting maps' accuracy obtained using the two classification methods for the combination datasets (S2 + S1 and L8 + S1). According to the tables, the mangrove class has the highest user accuracy among the four land cover classes based on the two algorithms used on the 3 datasets; that is, the user accuracies of the mangrove class for SVM and RF algorithms related to the data (L8 + S1) are 100 and 96.30, respectively, while the user accuracies of the mangrove class related to dataset S2 + S1 are 100 and 93.55 for the SVM algorithm and the RF algorithm, respectively. Also, both classification methods in optical and radar satellite datasets had good performance in differentiating other classes (user accuracy above 81% for water, mud, and tidal land classes). The manufacturer's accuracy follows the same patterns for evaluating each class. The SVM and RF datasets (S2 + S1) are 95.79 and 92.43, respectively, and the accuracies of the SVM and RF datasets (L8 + S1) are 91.52 88.98, respectively. The kappa coefficients of the SVM algorithm for the datasets (S2 + S1) and (L8 + S1) are 0.94 and 0.88, respectively. The kappa coefficients of the RF algorithm for the datasets (S2 + S1) and (L8 + S1) are 0.89 and 0.85%, respectively.

Figures 4 and 5 illustrate the maps obtained from SVM and RF classifications of Optical and SAR datasets. As shown in the selected section of the S2 + S1 and L8 + S1 maps by the SVM algorithm, this algorithm, in addition to the acceptable classification of mangrove lands, has been able to distinguish well in both satellite scenarios of mud lands and tidal lands. However, the selected section in the S2 + S1 and L8 + S1 maps, classified by the RF algorithm, could not distinguish between tidal, mud lands, and sea. It has a potent mix of mud classes and tidal lands.

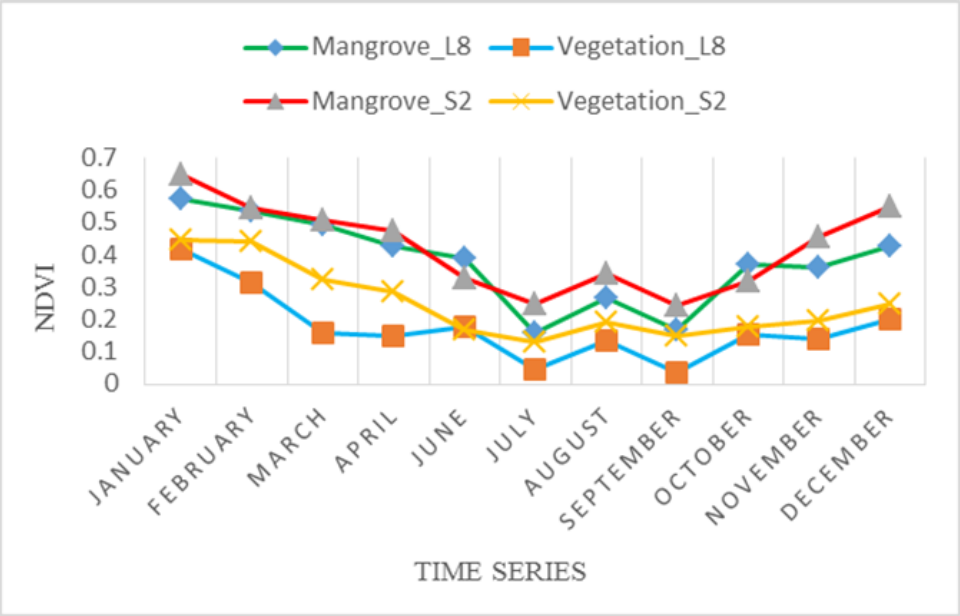

Figure 3. Comparing the average time-series images of NDVI for mangrove cover and typical vegetation cover in Landsat-8 and Sentinel-2

Table 3. The parameters of matrix for algorithms

Classification/Satellite	class	Mangrove	Mud	Tidal Zone	Sea	PA	UA
SVM-Sentinel2+Sentinel1	Mangrove	96.55	0	0	0	96.55	100
	Mud	3.45	100	0	0	100	96.77
	Tidal	0	0	96.67	10	96.67	90.63
	Sea	0	0	3.33	90	90	96.43
	Overall Accuracy = 95.79						
	Kappa Coefficient = 0.94						
RF-Sentinel2+Sentinel1	Mangrove	100	6.67	0	0	100	93.55
	Mud	0	93.33	0	0	93.33	100
	Tidal	0	0	93.33	16.67	93.33	84.85
	Sea	0	0	6.67	83.33	83.33	92.59
	Overall Accuracy = 92.43%						
	Kappa Coefficient = 0.89						
SVM-Landsat-8+Sentinel1	Mangrove	92.86	0	0	0	92.86	100
	Mud	7.14	100	0	3.33	100	90.91
	Tidal	0	0	96.67	20	96.67	82.86
	Sea	0	0	3.33	76.67	76.67	95.83
	Overall Accuracy = 91.52%						
	Kappa Coefficient = 0.88						
RF-Landsat-8+Sentinel1	Mangrove	92.86	3.33	0	0	92.86	96.30
	Mud	7.14	96.67	0	0	96.67	93.55
	Tidal	0	0	96.67	20	86.67	81.25
	Sea	0	0	3.33	80	80	85.71
	Overall Accuracy = 88.98%						
	Kappa Coefficient = 0.85						

3.3. Comparison of land cover area

Despite the increased improvement of map accuracy through combining radar and optics data in two machine learning methods (user accuracy greater than 81%), the resulting land cover maps differ in terms of area (Figure 6). As shown in Figure 6, the area of the land cover map obtained from the SVM algorithm for the combined dataset of Sentinel-2 and Sentinel-1 (mangrove area: 8333.41, mudflat: 25265.34, tidal areas: 13204.44, and sea: 27707.19 hectares) was nearly comparable with the area of the land cover map obtained from Landsat- 8 and Sentinel-1 datasets (mangrove area: 8544.72, mudflat: 24702.54, tidal areas: 12472.46 and sea: 287911.08 hectares).

However, the map obtained from the Landsat-8 and Sentinel-1 combination datasets based on the RF algorithm yielded a smaller estimate of the area of mangrove forests (7305.25 ha) compared to that obtained by the Sentinel-2 and Sentinel-1 datasets. The area of other lands based on RF algorithm in Sentinel-2 and Sentinel-1 combination datasets (mud area: 24674.31, tidal areas: 14051.36 and sea: 27209.9 hectares, respectively) gave results somewhat similar to those obtained from Landsat- 8 and Sentinel-1 combination datasets (244.85 mud area): Tidal zones: 12477.64, sea: 30301.07), but this classification method did not yield a better result compared to the SVM algorithm.

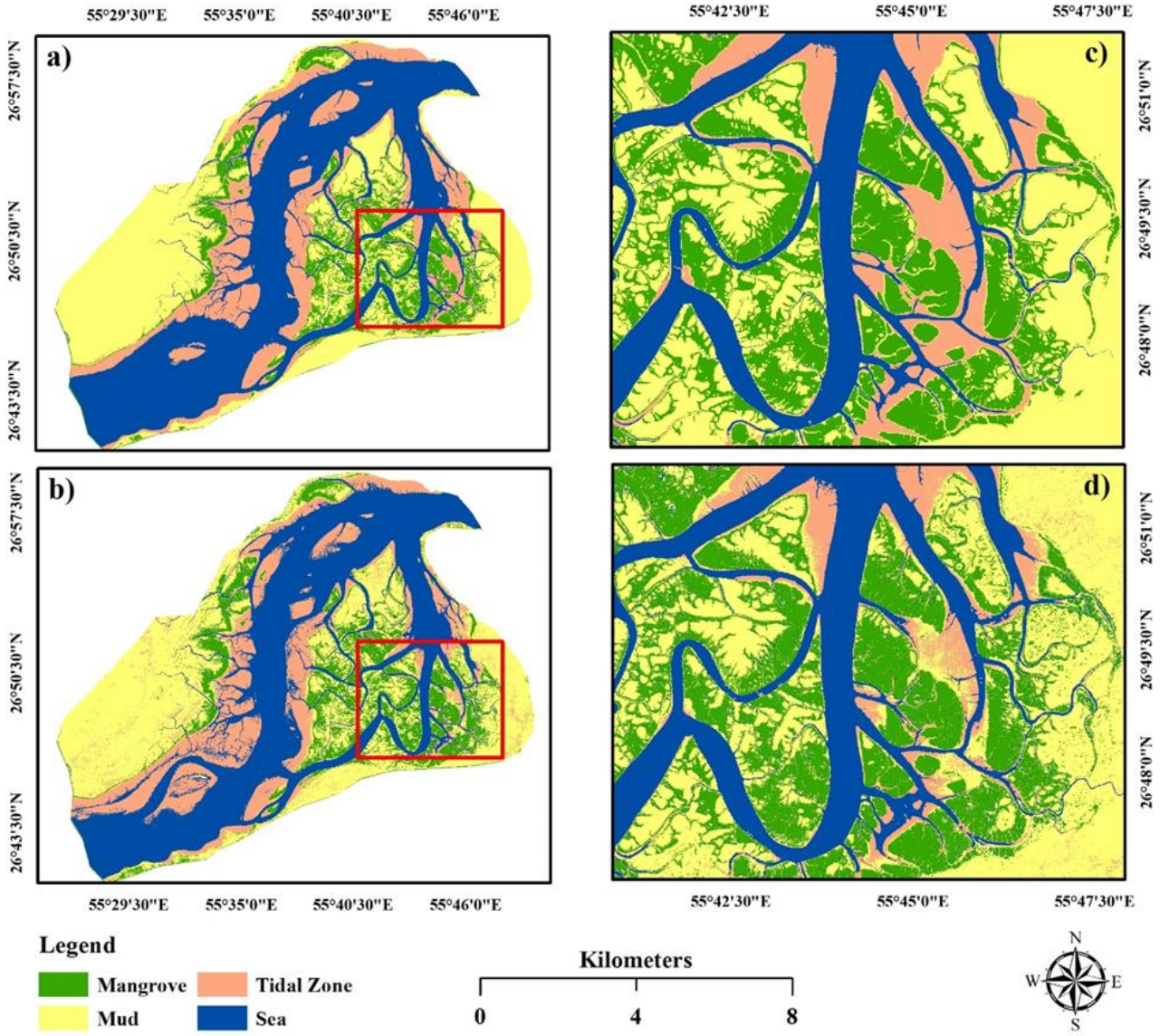

Figure 4 .Land cover map based on SVM algorithm related to S2 + S1 (a) combination dataset, SVM land cover map of S2 + S1 database in zoom-out mode (c), Land cover map based on RF algorithm related to S2 + S1 (b) combination database RF land cover data set S2 + S1 in zoom-out mode (d)

4. Discussion and Conclusion

This study aims to use a combination of optical and radar datasets (Landsat- 8 + Sentinel-and Sentinel-2 + Sentinel-1) to improve the accuracy of land cover maps and compare and assess them. Given the objectives of this study, the land cover was mapped using the new Google Earth Engine processor. Mondal et al. [23] used CART and RF machine learning algorithms to map mangrove forests. They stated that the accuracy of the maps obtained from the used algorithms is more than 90%, while in the current study, the land cover maps prepared based on the RF algorithm in GEE had an accuracy of less than 91%. Dong et al. [24] integrated the Sentinel-1 and Sentinel-2 images in the GEE to differentiate the Spartina alterniflora from the mangrove. Their results show that the combination of optics and radar data improved the accuracy of classified maps by about 99%. This theory is entirely consistent with our study because the use of a combination of optics and radar data in both 30-meter and 10-meter images has resulted in better differentiation of the mangrove class from other land covers. Jahanbakhshi and Ekhtesasi [59] Applied SVM and RF algorithms to vegetation classification and land use. They concluded that the SVM algorithm is more valuable, providing logical results that confirm the current study results. Zhen et al. [2] used SAR data in the C and Landsat-8 bands to develop a suitable method for improving the classification of mangrove forests. Their results showed that the combination of optical data with radar yields an overall accuracy of up to 95%, confirming the current study results regarding the combination of Sentinel-1 and Sentinel-2 (SVM) and the overall accuracy of 95% resulting from such a combination. In general, managers and planners usually require frequent and regular monitoring of marine ecosystems such as mangrove forests monthly or annually. Such monitoring requires a large amount of satellite data and a powerful hardware system, which the GEE system has provided in recent years. EGG includes large amounts of satellite data (such as Landsat-8, Sentinel-2, and Sentinel-1) and advanced machine learning algorithms such as RF and SVM in the cloud and is available completely free. For this purpose, a

combination of free satellite data categorized as radar and optical data has improved land cover classification in the cloud-based GEE. Given the objectives of the present study, hybrid satellite data (Landsat-8 + Sentinel-1 and Sentinel-2 + Sentinel-1), SVM, and RF machine learning algorithms were used in the GEE. Due to their high spectral power and strong interpretation, optical data can achieve better classification results but requires more accurate spatial information concerning the biophysical properties of vegetation, which has been estimated by radar. In this study, the combined optical and radar variables (NDVI index, NDWI, and VH redistribution) helped improve the algorithms' results. This suggests that optical and radar properties can be combined to map mangrove forests using machine learning algorithms such as RF and SVM. In other words, radar data eliminates the problems of optical sensing and improves the classification accuracy of thematic maps, especially mangrove mapping, when combined with optical data. In this study, the SVM algorithm in both combination datasets of Landsat-8 + Sentinel1 and Sentinel-2 + Sentinel-1 showed a very reasonable and good result compared to similar use of datasets with RF algorithm. This means that the SVM algorithm is one of the most desirable machine learning algorithms used in land use classification and land use. Thus, based on the results of this study, we recommend using the GEE system and other advanced machine learning algorithms in the cloud space to process time-series data for mapping the land cover. Moreover, it is better to use machine learning algorithms from radar data in-band L for achieving relevant results with high accuracy of 95% due to the very high penetration of such data up to about 25 cm in vegetation.

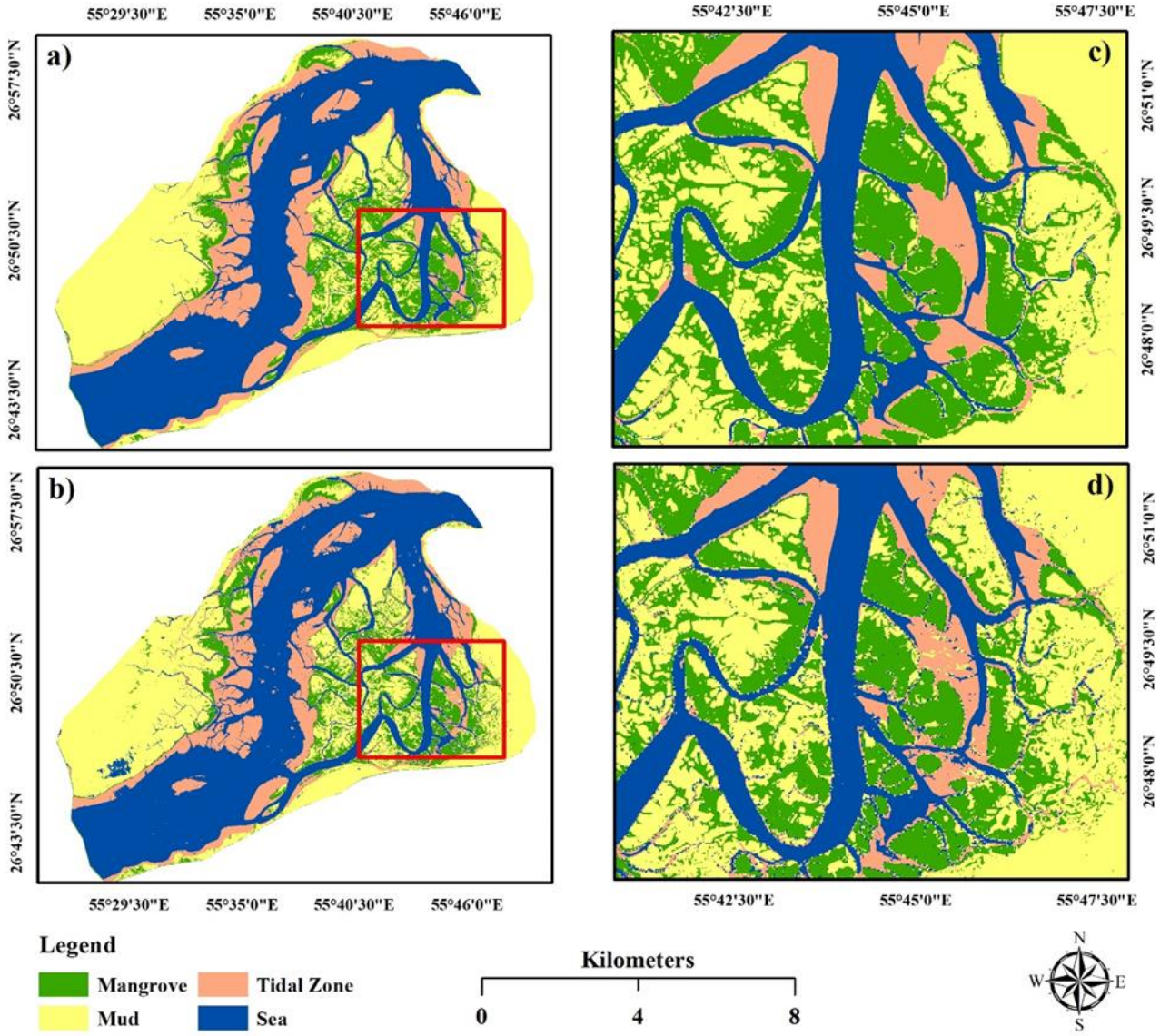

Figure 5. Land cover map based on SVM algorithm related to L8 + S1 (a) combination dataset, SVM land cover map of L8 + S1 combination dataset in zoom-out mode (c), Land cover map based on RF algorithm related to L8 + S1 (b) combination dataset RF land cover data set L8 + S1 in zoom-out mode (d),

Figure 6. Comparing the area of land cover in combination dataset based on different machine learning algorithms

Author contributions

Mostafa Mahdavifard: Methodology, Data Collection, Image Processing, Validation **Sara Kaviani**: Writing-Original draft preparation, Reviewing and Editing. **Bakhtiar Feizizadeh**: Optic processing **Khalil Valizadeh Kamran:** Mangrove and Optic processing **Sadra Karimzadeh:** SAR processing.

Conflicts of interest

The authors declare no conflicts of interest.

References

1. Giri, C., Long, J., Abbas, S., Murali, R. M., Qamer, F. M., Pengra, B., & Thau, D. (2015). Distribution and dynamics of mangrove forests of South Asia. *Journal of environmental management*, *148*, 101-111.
2. Zhen, J., Liao, J., & Shen, G. (2018). Mapping mangrove forests of Dongzhaigang nature reserve in China using Landsat 8 and Radarsat-2 polarimetric SAR data. *Sensors*, *18*(11), 4012.
3. Collins, D. S., Avdis, A., Allison, P. A., Johnson, H. D., Hill, J., Piggott, M. D., ... & Damit, A. R. (2017). Tidal dynamics and mangrove carbon sequestration during the Oligo–Miocene in the South China Sea. *Nature communications*, *8*(1), 15698.
4. Jia, M., Wang, Z., Wang, C., Mao, D., & Zhang, Y. (2019). A new vegetation index to detect periodically submerged mangrove forest using single-tide Sentinel-2 imagery. *Remote Sensing*, *11*(17), 2043.
5. Gupta, K., Mukhopadhyay, A., Giri, S., Chanda, A., Majumdar, S. D., Samanta, S., ... & Hazra, S. (2018). An index for discrimination of mangroves from non-mangroves using LANDSAT 8 OLI imagery. *MethodsX*, *5*, 1129-1139.
6. Vaiphasa, C. (2006). *Remote sensing techniques for mangrove mapping*. Doctoral Dissertation, Wageningen University and Research.
7. Danehkar, A., Jalali, S.G., 2005. Avicennia marina forest structure using line plot method. Pajouhesh and Sazandegi 67, 18–24
8. Cárdenas, N. Y., Joyce, K. E., & Maier, S. W. (2017). Monitoring mangrove forests: Are we taking full advantage of technology?. *International Journal of Applied Earth Observation and Geoinformation*, *63*, 1-14.
9. Long, B. G., & Skewes, T. D. (1996). A technique for mapping mangroves with Landsat TM satellite data and geographic information system. *Estuarine, Coastal and Shelf Science*, *43*(3), 373-381.
10. Long, J. B., & Giri, C. (2011). Mapping the Philippines' mangrove forests using Landsat imagery. *Sensors*, *11*(3), 2972-2981.
11. Pasqualini, V., Iltis, J., Dessay, N., Lointier, M., Guelorget, O., & Polidori, L. (1999). Mangrove mapping in North-Western Madagascar using SPOT-XS and SIR-C radar data. *Hydrobiologia*, *413*, 127-133.
12. Hu, L., Xu, N., Liang, J., Li, Z., Chen, L., & Zhao, F. (2020). Advancing the mapping of mangrove forests at national-scale using Sentinel-1 and Sentinel-2 time-series data with Google Earth Engine: A case study in China. *Remote Sensing*, *12*(19), 3120.
13. Zhu, X., Meng, L., Zhang, Y., Weng, Q., & Morris, J. (2019). Tidal and meteorological influences on the growth of invasive Spartina alterniflora: evidence from UAV remote sensing. *Remote Sensing*, *11*(10), 1208.
14. Tarantino, C., Casella, F., Adamo, M., Lucas, R., Beierkuhnlein, C., & Blonda, P. (2019). Ailanthus altissima mapping from multi-temporal very high

resolution satellite images. *ISPRS Journal of Photogrammetry and Remote Sensing*, *147*, 90-103.
15. Campbell, A. D., & Wang, Y. (2020). Salt marsh monitoring along the mid-Atlantic coast by Google Earth Engine enabled time series. *PloS one*, *15*(2), e0229605.
16. Fonteh, M. L., Theophile, F., Cornelius, M. L., Main, R., Ramoelo, A., & Cho, M. A. (2016). Assessing the utility of sentinel-1 c band synthetic aperture radar imagery for land use land cover classification in a tropical coastal systems when compared with landsat 8. *Journal of Geographic Information System*, *8*(4), 495-505.
17. Zhu, Y., Liu, K., Liu, L., Wang, S., & Liu, H. (2015). Retrieval of mangrove aboveground biomass at the individual species level with worldview-2 images. *Remote Sensing*, *7*(9), 12192-12214.
18. Zhen, J., Liao, J., & Shen, G. (2018). Mapping mangrove forests of Dongzhaigang nature reserve in China using Landsat 8 and Radarsat-2 polarimetric SAR data. *Sensors*, *18*(11), 4012.
19. Carrasco, L., O'Neil, A. W., Morton, R. D., & Rowland, C. S. (2019). Evaluating combinations of temporally aggregated Sentinel-1, Sentinel-2 and Landsat 8 for land cover mapping with Google Earth Engine. *Remote Sensing*, *11*(3), 288.
20. Gorelick, N., Hancher, M., Dixon, M., Ilyushchenko, S., Thau, D., & Moore, R. (2017). Google Earth Engine: Planetary-scale geospatial analysis for everyone. *Remote sensing of Environment*, *202*, 18-27.
21. Shrestha, S., Miranda, I., Kumar, A., Pardo, M. L. E., Dahal, S., Rashid, T., ... & Mishra, D. R. (2019). Identifying and forecasting potential biophysical risk areas within a tropical mangrove ecosystem using multi-sensor data. *International Journal of Applied Earth Observation and Geoinformation*, *74*, 281-294.
22. Diniz, C., Cortinhas, L., Nerino, G., Rodrigues, J., Sadeck, L., Adami, M., & Souza-Filho, P. W. M. (2019). Brazilian mangrove status: Three decades of satellite data analysis. *Remote Sensing*, *11*(7), 808.
23. Mondal, P., Liu, X., Fatoyinbo, T. E., & Lagomasino, D. (2019). Evaluating combinations of sentinel-2 data and machine-learning algorithms for mangrove mapping in West Africa. *Remote Sensing*, *11*(24), 2928.
24. Dong, D., Wang, C., Yan, J., He, Q., Zeng, J., & Wei, Z. (2020). Combing Sentinel-1 and Sentinel-2 image time series for invasive Spartina alterniflora mapping on Google Earth Engine: A case study in Zhangjiang Estuary. *Journal of Applied Remote Sensing*, *14*(4), 044504.
25. Pham, T. D., & Yoshino, K. (2015, March). Mangrove mapping and change detection using multi-temporal Landsat imagery in Hai Phong city, Vietnam. In *International symposium on cartography in internet and ubiquitous environments* (pp. 17-19).
26. Shi, T., Liu, J., Hu, Z., Liu, H., Wang, J., & Wu, G. (2016). New spectral metrics for mangrove forest identification. *Remote Sensing Letters*, *7*(9), 885-894.
27. Pimple, U., Simonetti, D., Sitthi, A., Pungkul, S., Leadprathom, K., Skupek, H., ... & Towprayoon, S. (2018). Google earth engine based three decadal landsat imagery analysis for mapping of mangrove forests and its surroundings in the trat province of Thailand. Journal of Computer and Communications, 6, 247-264
28. Gessesse, A. A., & Melesse, A. M. (2019). Temporal relationships between time series CHIRPS-rainfall estimation and eMODIS-NDVI satellite images in Amhara Region, Ethiopia. In *Extreme hydrology and climate variability* (pp. 81-92). Elsevier.
29. Ghorbanian, A., Zaghian, S., Asiyabi, R. M., Amani, M., Mohammadzadeh, A., & Jamali, S. (2021). Mangrove ecosystem mapping using Sentinel-1 and Sentinel-2 satellite images and random forest algorithm in Google Earth Engine. *Remote Sensing*, *13*(13), 2565.
30. Huang, K., Yang, G., Yuan, Y., Sun, W., Meng, X., & Ge, Y. (2022). Optical and SAR images Combined Mangrove Index based on multi-feature fusion. *Science of Remote Sensing*, *5*, 100040.
31. Shen, Z., Miao, J., Wang, J., Tang, A., & Zhen, J. (2023). Combining Optical and Sar Data for Mapping Mangrove Forests Using Feature Selection and Machine Learning Methods. SSRN
32. Bihamta Toosi, N., Soffianian, A. R., Fakheran, S., Pourmanafi, S., Ginzler, C., & T. Waser, L. (2020). Land cover classification in mangrove ecosystems based on VHR satellite data and machine learning—an upscaling approach. *Remote Sensing*, *12*(17), 2684.
33. Worthington, T. A., Zu Ermgassen, P. S., Friess, D. A., Krauss, K. W., Lovelock, C. E., Thorley, J., ... & Spalding, M. (2020). A global biophysical typology of mangroves and its relevance for ecosystem structure and deforestation. *Scientific reports*, *10*(1), 1-11.
34. Walker, W. (2014). Introduction to RADAR Remote Sensing for Vegetation Mapping and Monitoring. *A Ph. D. presentation: Woods Hole Research Center*, *22*.
35. Baghdadi, N., El Hajj, M., Zribi, M., & Bousbih, S. (2017). Calibration of the water cloud model at C-band for winter crop fields and grasslands. *Remote Sensing*, *9*(9), 969.
36. Vrieling, A., De Leeuw, J., & Said, M. Y. (2013). Length of growing period over Africa: Variability and trends from 30 years of NDVI time series. *Remote sensing*, *5*(2), 982-1000.
37. Tucker, C. J. (1979). Red and photographic infrared linear combinations for monitoring vegetation. *Remote sensing of Environment*, *8*(2), 127-150.
38. Zhu, Z., Bi, J., Pan, Y., Ganguly, S., Anav, A., Xu, L., ... & Myneni, R. B. (2013). Global data sets of vegetation leaf area index (LAI) 3g and fraction of photosynthetically active radiation (FPAR) 3g derived from global inventory modeling and mapping studies (GIMMS) normalized difference vegetation index (NDVI3g) for the period 1981 to 2011. *Remote sensing*, *5*(2), 927-948.
39. Viana, C. M., Oliveira, S., Oliveira, S. C., & Rocha, J. (2019). Land use/land cover change detection and urban sprawl analysis. In *Spatial modeling in GIS and R for earth and environmental sciences* (pp. 621-651). Elsevier.
40. Javadnia, E., Mobasheri, M. R., & Kamali, G. A. (2009). MODIS NDVI quality enhancement using ASTER images. Journal of Agricultural Science and Technology, 11, 549-558.

41. McFeeters, S. K. (1996). The use of the Normalized Difference Water Index (NDWI) in the delineation of open water features. *International journal of remote sensing*, *17*(7), 1425-1432.
42. Jensen, J. R. (1996). *Introductory digital image processing: a remote sensing perspective* (No. Ed. 2). Prentice-Hall Inc..
43. Schulz, K., Hänsch, R., & Sörgel, U. (2018). Machine learning methods for remote sensing applications: an overview. *Earth resources and environmental remote sensing/GIS applications IX*, *10790*, 1079002.
44. Liu, K., Li, X., Shi, X., & Wang, S. (2008). Monitoring mangrove forest changes using remote sensing and GIS data with decision-tree learning. *Wetlands*, *28*, 336-346.
45. Heumann, B. W. (2011). An object-based classification of mangroves using a hybrid decision tree—Support vector machine approach. *Remote Sensing*, *3*(11), 2440-2460.
46. Feizizadeh, B., Omarzadeh, D., Kazemi Garajeh, M., Lakes, T., & Blaschke, T. (2023). Machine learning data-driven approaches for land use/cover mapping and trend analysis using Google Earth Engine. *Journal of Environmental Planning and Management*, *66*(3), 665-697.
47. Torres, M., & Qiu, G. (2014). Automatic habitat classification using image analysis and random forest. *Ecological informatics*, *23*, 126-136.
48. Fu, B., Wang, Y., Campbell, A., Li, Y., Zhang, B., Yin, S., ... & Jin, X. (2017). Comparison of object-based and pixel-based Random Forest algorithm for wetland vegetation mapping using high spatial resolution GF-1 and SAR data. *Ecological indicators*, *73*, 105-117.
49. Millard, K., & Richardson, M. (2015). On the importance of training data sample selection in random forest image classification: A case study in peatland ecosystem mapping. *Remote sensing*, *7*(7), 8489-8515.
50. Phan, T. N., Kuch, V., & Lehnert, L. W. (2020). Land cover classification using Google Earth Engine and random forest classifier—The role of image composition. *Remote Sensing*, *12*(15), 2411.
51. Amani, M., Mahdavi, S., Afshar, M., Brisco, B., Huang, W., Mohammad Javad Mirzadeh, S., ... & Hopkinson, C. (2019). Canadian wetland inventory using Google Earth Engine: The first map and preliminary results. *Remote Sensing*, *11*(7), 842.
52. Tappan, G. G., Sall, M., Wood, E. C., & Cushing, M. (2004). Ecoregions and land cover trends in Senegal. *Journal of arid environments*, *59*(3), 427-462.
53. Mountrakis, G., Im, J., & Ogole, C. (2011). Support vector machines in remote sensing: A review. *ISPRS journal of photogrammetry and remote sensing*, *66*(3), 247-259.
54. Toosi, N. B., Soffianian, A. R., Fakheran, S., Pourmanafi, S., Ginzler, C., & Waser, L. T. (2019). Comparing different classification algorithms for monitoring mangrove cover changes in southern Iran. *Global Ecology and Conservation*, *19*, e00662.
55. Andrew, A. M. (2000). An Introduction to Support Vector Machines and Other Kernel-Based Learning Methods by Nello Christianini and John Shawe-Taylor, Cambridge University Press, Cambridge, 2000, xiii+ 189 pp., ISBN 0-521-78019-5 (Hbk,£ 27.50). *Robotica*, *18*(6), 687-689.
56. Ding, H. Y., & Bian, Z. F. (2008). Theory of support vector machine and its applications in remote sensing image processing. Computer *Engineering Design*, *5*, 62.
57. Foody, G. M. (2020). Explaining the unsuitability of the kappa coefficient in the assessment and comparison of the accuracy of thematic maps obtained by image classification. *Remote Sensing of Environment*, *239*, 111630.
58. Mohammadi, A., Karimzadeh, S., Valizadeh Kamran, K., & Matsuoka, M. (2020). Extraction of land information, future landscape changes and seismic hazard assessment: A case study of Tabriz, Iran. *Sensors*, *20*(24), 7010.
59. Jahanbakhshi, F., & Ekhtesasi, M. R. (2019). Performance evaluation of three image classification methods (Random Forest, Support Vector Machine and the Maximum Likelihood) in land use mapping. *Journal of Water and Soil Science*, *22*(4), 235-247